ACI STRUCTURAL JOURNAL TECHNICAL PAPER

Title No. 113-S68

# Strut Efficiency-Based Design for Concrete Deep Beams Reinforced with Fiber-Reinforced Polymer Bars

by Khaled Mohamed, Ahmed Sabry Farghaly, and Brahim Benmokrane

*In this paper, a strut-and-tie-based model is proposed to predict the shear strength of fiber-reinforced polymer-reinforced (FRP) deep beams. An assessment of the available strut-and-tie models (STMs) in ACI and CSA provisions was conducted, identifying the important parameters affecting the strut efficiency factor. The tendency of each parameter (concrete compressive strength, shear span-depth ratio, and strain in longitudinal reinforcement) was assessed against the efficiency factor. The data from the 28 specimens with and without web reinforcement, including 12 tested FRP-reinforced concrete deep beams in our study and 16 FRP-reinforced deep beams taken from the literature, were used to assess the proposed model. The model was capable of capturing the failure mode and predicting the ultimate capacity of the tested FRP-reinforced deep beams. The proposed model was verified against a compilation of databases on 172 steel-reinforced deep beams, resulting in an acceptable level of adequacy.*

**Keywords:** deep beams; efficiency factor; fiber-reinforced polymer (FRP) bars; shear strength; strut-and-tie model (STM).

## INTRODUCTION

Deep beams have relatively small span-depth ratios ($a/d$), so that shear strain becomes dominant. Hence, traditional sectional design approaches based on plane sectional theory is not applicable for the design of deep beams, in which the plane section does not remain plane, thereby requiring a different approach. In deep beams, externally applied loads are transferred directly to the supports by strut action (MacGregor 1997). As a result, provisions—such as in ACI and CSA—recommend the use of strut-and-tie model (STM) for designing reinforced-concrete deep beams.

The strut-and-tie model idealizes the complex flow of stresses using a pin-jointed truss consisting of compression struts and tension ties, which allows for easier monitoring of the force flow (Schlaich et al. 1987). The STM can only be applied to an element, however, if the truss model follows the lower-bound theorem, under which the capacity of a STM is always lower than the structure's actual capacity. If the truss model is in equilibrium, the truss will exhibit the deformation capacity required to redistribute the internal stresses and the stresses applied to the STM elements within their limit capacity.

In practice, deep beams are commonly used when designing transfer girders or bridge bents. These elements are exposed to aggressive environments in northern climates, which causes the steel bars to corrode. So, researchers have examined the use of fiber-reinforced polymer (FRP) instead of steel as internal reinforcement in deep beams (Andermatt and Lubell 2013a,b; Farghaly and Benmokrane 2013). The tested FRP-reinforced deep beams demonstrated sufficient deformability to distribute the stresses according to the STM. CSA S806 (2012) introduced the STM for FRP-reinforced deep beams, which is the same model specified in CSA A23.3 (2014) for steel-reinforced deep beams, although the STM was not used in ACI 440.1R (2006). Therefore, our study aimed at assessing the factors affecting the efficiency of the concrete strut and at developing a new STM based on the tested FRP-reinforced deep beams.

## RESEARCH SIGNIFICANCE

The strut-and-tie design models provided in ACI 318 (2011) and CSA S806 (2012) provisions were assessed and found to be unsatisfactory because they disregard the contribution of major strength-related parameters. The effect of the different strength-related parameters on the strut efficiency factor was assessed based on the experimental results in the literature and that from our experimental program. A new strut efficiency factor for the STM-based procedure was proposed and validated with the FRP- and steel-reinforced deep beams.

## SUMMARY OF EXPERIMENTAL RESULTS

Twelve full-scale reinforced-concrete deep beams entirely reinforced with GFRP bars were constructed and tested to failure under two-point loading with different shear span-depth ratios ($a/d$) of 1.47, 1.13, and 0.83. Figure 1(a) shows the concrete dimensions and the reinforcement details of the tested specimens, while Fig. 1(b) provides the loading setup. The amount of web reinforcement was chosen to satisfy ACI 318 (2011) and CSA S806 (2012) requirements. Tables 1 and 2 present the material properties and reinforcement details, respectively.

The failure of all specimens was preceded by crushing in the concrete diagonal strut, which is the typical failure of deep beams (Fig. 2). The tested specimens exhibited reasonable deflection levels compared to the available information found in the literature (Mihaylov et al. 2010) on steel-reinforced deep beams with similar dimensions and reinforcement. The development of arch action was also confirmed through the almost constant strain distribution along the longitudinal reinforcement length, as shown in Fig. 3.

All web reinforcement configurations used in the tested specimens yielded insignificant effects on the ultimate strength, as given in Table 3. The test results were used to assess the STMs in ACI 318 (2011) and CSA S806 (2012).

*ACI Structural Journal*, V. 113, No. 4, July-August 2016.
MS No. S-2015-064.R2, doi: 10.14359/51688476, was received July 26, 2015, and reviewed under Institute publication policies. 

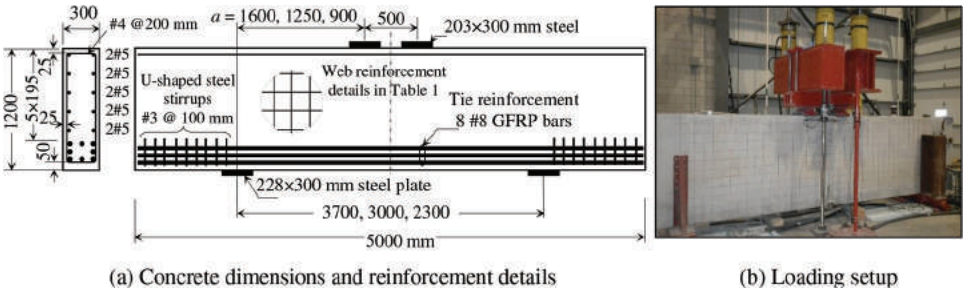


*Fig. 1—Concrete dimensions, reinforcement details, and loading setup. (Note: Dimensions in mm; 1 mm = 0.0394 in.)*

**Table 1—Tensile properties of GFRP bars as reported by manufacturer**

| Bar diameter $\varnothing_f$*, mm | Nominal cross-sectional area $A_f$, mm$^2$ | Guaranteed tensile strength $f_{fu}$†, MPa | Modulus of elasticity $E_{frp}$, GPa |
|---|---|---|---|
| 13 (No. 4) | 1299 | 941 | 53.6 |
| 15 (No. 5) | 199 | 1184 | 62.6 |
| 25 (No. 8) | 510 | 1000 | 62.4 |

*Numbers in parentheses are manufacturer's bar designation.

†Guaranteed tensile strength; average value is 3× standard deviation (ACI 440.1R-06).

Notes: 1 mm = 0.0394 in.; 1 MPa = 145 psi.

**Table 2—Reinforcement details**

| Specimen ID | $a/d$ | Longitudinal bars | | Web bars | | | |
|---|---|---|---|---|---|---|---|
| | | No. of bars | $d_b$ | Vertical | | Horizontal | |
| | | | | $d_b$ | $s_v$ | $d_b$ | $s_h$ |
| G1.47 | 1.47 | 8 | 25 (No. 8) | — | — | — | — |
| G1.47H | | | | — | — | 16 (No. 5) | 195 |
| G1.47V | | | | 12.7 (No. 4) | 200 | — | — |
| G1.13 | 1.13 | | | — | — | — | — |
| G1.13H | | | | — | — | 16 (No. 5) | 195 |
| G1.13V | | | | 12.7 (No. 4) | 200 | — | — |
| G1.13VH | | | | 12.7 (No. 4) | 200 | 16 (No. 5) | 195 |
| G0.83 | 0.83 | | | — | — | — | — |
| G0.83H | | | | — | — | 16 (No. 5) | 195 |
| G0.83V | | | | 12.7 (No. 4) | 200 | — | — |
| SG1.13 | 1.13 | | | — | — | — | — |
| SG1.13VH | | | | 12.7 (No. 4) | 200 | 16 (No. 5) | 195 |

Notes: $d_b$ is bar diameter, mm; $s_v$ is spacing between vertical web bars, mm; $s_h$ is spacing between horizontal web bars, mm; 1 mm = 0.0394 in.

## STRUT-AND-TIE MODEL

The strut-and-tie model (STM) is an approach used to design discontinuity regions (D-regions) in reinforced-concrete structures to reduce the complex states of stress into a truss comprised of simple, uniaxial stress paths (Fig. 4). The members of the STM subjected to tensile stresses are called ties and represent the location where reinforcement should be placed, while the members subjected to compression are called struts. The points where truss members intersect are called nodes. Most design specifications recognize three major node types: CCC nodes (bounded by struts only), CCT nodes (bounded by one tie and two or more struts), and CTT nodes (bounded by one strut and two or more ties). If the forces acting on STM boundaries are known, the forces in each of the truss members can be determined using basic truss theory.

The ACI and CSA STM design provisions allow the use of any truss configuration according to designer provisions. In general, the one-panel STM shown in Fig. 4 was found to be the preferred mechanism in steel-reinforced deep beams with a limited amount of web reinforcement (Brown and Bayrak 2006) and was therefore applied to the tested FRP-reinforced deep beams.

Defining the geometry of the nodal regions involves calculating stresses on struts and nodal faces as follows

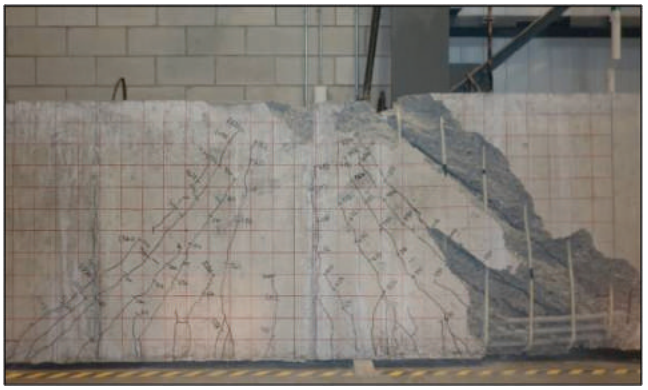

*Fig. 2—Typical crushing-failure mode (G1.13V).*

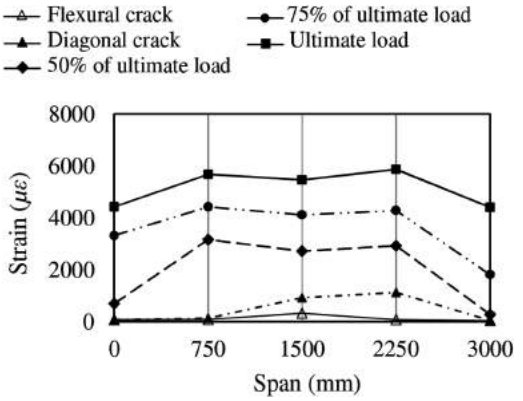


*Fig. 3—Typical strain distribution (G1.13). (Note: 1 mm = 0.0394 in.)*

**Table 3—Capacity prediction of tested FRP-reinforced deep beams**

| Specimen ID | | $b$, mm | $d$, mm | $l_{b1}$, mm | $l_{b2}$, mm | $f_c'$, MPa | $A_{frp}$, mm$^2$ | $E_{frp}$, GPa | $P_{exp}$, kN | ACI 318 $P_{exp}/P_{pred}$ | CSA S806 $P_{exp}/P_{pred}$ | Proposed model $P_{exp}/P_{prop}$ |
|---|---|---|---|---|---|---|---|---|---|---|---|---|
| Authors | G1.47 | 300 | 1088 | 232 | 203 | 38.7 | 4054 | 66.4 | 1849 | 0.98 | 2.48 | 1.08 |
| | G1.47H | 300 | 1088 | 232 | 203 | 45.4 | 4054 | 66.4 | 1695 | 0.64 | 2.05 | 1.10 |
| | G1.47V | 300 | 1088 | 232 | 203 | 45.4 | 4054 | 66.4 | 2650 | 1.00* | 1.15* | 1.04* |
| | G1.13 | 300 | 1088 | 232 | 203 | 37.0 | 4054 | 66.4 | 2687 | 1.22 | 2.35 | 1.05 |
| | G1.13H | 300 | 1088 | 232 | 203 | 44.6 | 4054 | 66.4 | 2533 | 0.78 | 1.97 | 0.98 |
| | G1.13V | 300 | 1088 | 232 | 203 | 44.6 | 4054 | 66.4 | 3236 | 1.23* | 1.45* | 1.15* |
| | G1.13VH | 300 | 1088 | 232 | 203 | 37.0 | 4054 | 66.4 | 2904 | 0.94* | 1.45* | 1.00* |
| | G0.83 | 300 | 1088 | 232 | 203 | 38.7 | 4054 | 66.4 | 3000 | 1.24 | 1.59 | 1.44 |
| | G0.83H | 300 | 1088 | 232 | 203 | 43.6 | 4054 | 66.4 | 3166 | 0.78 | 1.56 | 1.05 |
| | G0.83V | 300 | 1088 | 232 | 203 | 43.6 | 4054 | 66.4 | 3387 | 0.83 | 1.67 | 1.08 |
| | SG1.13 | 300 | 1088 | 232 | 203 | 43.1 | 3928 | 66.0 | 2928 | 1.15 | 2.44 | 1.15 |
| | SG1.13VH | 300 | 1088 | 232 | 203 | 43.1 | 3928 | 66.0 | 3110 | 1.11* | 1.41* | 1.10* |
| Farghaly and Benmokrane (2013) | G6#8 | 300 | 1097 | 232 | 130 | 49.3 | 2280 | 47.6 | 1477 | 0.75 | 1.96 | 0.98 |
| | G8#8 | 300 | 1088 | 232 | 130 | 49.3 | 4054 | 51.9 | 1906 | 0.97 | 1.97 | 1.15 |
| | C12#3 | 300 | 1111 | 232 | 130 | 38.7 | 856 | 120.0 | 1191 | 0.77 | 1.83 | 1.08 |
| | C12#4 | 300 | 1106 | 232 | 130 | 38.7 | 1520 | 144.0 | 1601 | 1.04 | 1.85 | 1.16 |
| Andermatt and Lubell (2013a) | A1N | 310 | 257 | 100 | 100 | 40.2 | 1188 | 41.1 | 814 | 1.00 | 1.86 | 1.23 |
| | A2N | 310 | 261 | 100 | 100 | 45.4 | 1188 | 41.1 | 472 | 0.66 | 1.68 | 1.31 |
| | A3N | 310 | 261 | 100 | 100 | 41.3 | 1188 | 41.1 | 244 | 0.55 | 1.89 | 1.65 |
| | A4N | 310 | 261 | 100 | 100 | 64.6 | 1188 | 41.1 | 192 | 0.22 | 1.13 | 1.14 |
| | B1N | 300 | 503 | 200 | 200 | 40.5 | 2576 | 37.9 | 1274 | 1.23 | 1.50 | 1.00 |
| | B2N | 300 | 501 | 200 | 200 | 39.9 | 2576 | 37.9 | 800 | 0.81 | 1.66 | 1.26 |
| | B3N | 300 | 502 | 200 | 200 | 41.2 | 2576 | 37.9 | 432 | 0.53 | 1.82 | 1.61 |
| | B4N | 300 | 496 | 200 | 200 | 40.7 | 3168 | 41.1 | 830 | 0.69 | 1.53 | 1.19 |
| | B5N | 300 | 497 | 200 | 200 | 66.4 | 3168 | 41.1 | 1062 | 0.54 | 1.44 | 1.32 |
| | B6N | 300 | 505 | 200 | 200 | 68.5 | 2576 | 37.9 | 376 | 0.27 | 1.14 | 1.18 |
| | C1N | 301 | 889 | 330 | 330 | 51.6 | 4224 | 42.3 | 2270 | 0.68 | 1.36 | 0.99 |
| | C2N | 304 | 891 | 330 | 330 | 50.7 | 4224 | 42.3 | 1324 | 0.53 | 1.38 | 1.15 |
| | | | | | | | | | Mean value | 0.83 | 1.77 | 1.17 |
| | | | | | | | | | COV, % | 34 | 25 | 15 |

*Based on two-panel truss model; $P_{exp}$ is ultimate load at failure recorded during testing; $P_{pred}$ is predicted load from ACI or CSA provisions; $P_{prop}$ is predicted load from proposed model; $l_{b1}$ is loading plate width; $l_{b2}$ is support plate width; all deep beams reinforced entirely with glass FRP bars, except C12#3 and C12#4, which were reinforced with carbon FRP bars.

Notes: 1 mm = 0.0394 in.; 1 MPa = 145 psi; 1 kN = 0.225 kip.

(Fig. 5). An iterative procedure would be used to calculate the capacity based on the condition of limiting the stresses acting on the truss components (struts, ties, and nodes) to their permitted allowable stress levels to satisfy the lower-bound theorem. The allowable design stress on struts and nodal faces ($f_{ce}$) varied according to the design provisions, as discussed in the following section.

### ACI 318 (2011) provisions

ACI 318 (2011) in Appendix A provides the STM-based design for deep beams. The nominal force carried by the strut is calculated as $F_{ns} = f_{ce} A_{cs}$; where $A_{cs}$ is the smaller cross-sectional area at either end of the strut and $f_{ce}$ is calculated as follows

$$f_{ce} = 0.85\beta_s f_c' \quad (1)$$

where $f_c'$ is the concrete compressive strength.

The strut efficiency factor $\beta_s$ depends on strut geometry, the reinforcement provided, and stress conditions in the member. For a strut of uniform cross-sectional area over its length, $\beta_s = 1.0$, while for a bottle-shaped strut, $\beta_s = 0.6$ when no web reinforcement is provided and $\beta_s = 0.75$ with reinforcement to satisfy the minimum web reinforcement specified as follows

$$\sum \frac{A_{si}}{bs_i} \sin \alpha_i \geq 0.003 \quad (2)$$

where $A_{si}$ is the reinforcement cross-sectional area crossing the strut in the $i$-th layer of reinforcement at spacing $s_i$ and angle $\alpha_i$ to the strut axis; and $b$ is the strut width perpendicular to the plane of the reinforcing bars.

Additionally, ACI 318 (2011) places limits on the allowable stresses at the node faces. The nominal force carried by the nodal zone is calculated as $F_{nn} = f_{ce} A_{nz}$; where $A_{nz}$ is the area of the nodal face; and $f_{ce}$ is calculated as follows

$$f_{ce} = 0.85 \beta_n f_c' \quad (3)$$

The value of the nodal efficiency factor $\beta_n$ in ACI 318 (2011) depends on the node boundary condition and is taken as equal to 1.0 for CCC nodal zones and 0.80 for CCT nodal zones.

## CSA S806 (2012) provisions

CSA S806 (2012) uses the STM to determine the internal forces in deep beams reinforced with FRP bars. The strut compressive force shall not exceed $f_{ce} A_{cs}$; where $A_{cs}$ is the effective cross-sectional area of the strut; and $f_{ce}$ is calculated based on the modified compression field theory (Vecchio and Collins 1986) as follows

$$f_{ce} = \frac{f_c'}{0.8 + 170\varepsilon_1} \quad (4)$$

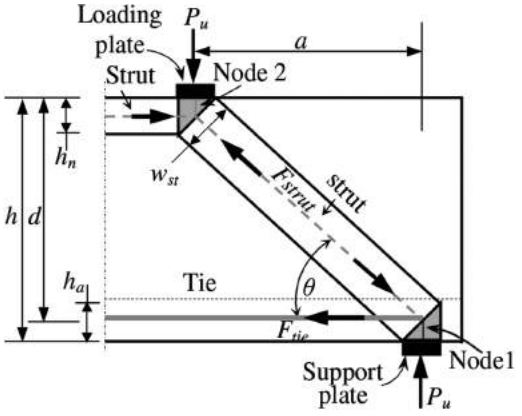


*Fig. 4—Strut-and-tie model (one-panel).*

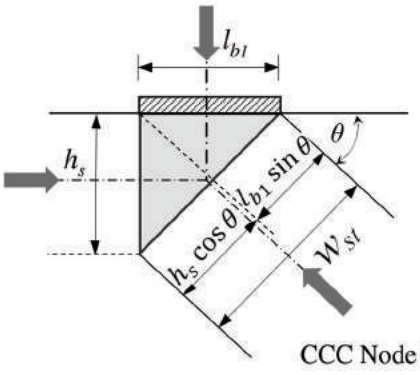


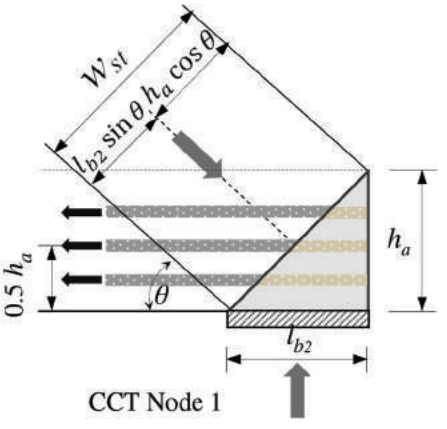


*Fig. 5—STM nodal geometry (one-panel).*

and

$$\varepsilon_1 = \varepsilon_{frp} + (\varepsilon_{frp} + 0.002) \cot^2 \theta \quad (5)$$

where $\varepsilon_{frp}$ is the tensile strain in the tie bar located closest to the tension face in the deep beam and inclined at an angle $\theta$ to the strut axis.

CSA S806 (2012) specifies that the stress limits in nodal zones shall not exceed $0.65\alpha f_c'$, where $\alpha$ depends on the nodal boundary conditions 0.85 in CCC nodes and 0.75 in CCT nodes. Moreover, the provision specifies a minimum web reinforcement ratio of 0.003 in each direction with a maximum spacing of 200 mm (7.87 in.) for crack control.

## Assessment of design provisions

The STM design provisions provided in ACI 318 (2011) and CSA S806 (2012) were used to calculate the capacity of the deep beams tested in our study as well as that of the FRP-reinforced deep beams taken from the literature (Farghaly and Benmokrane 2013; Andermatt and Lubell 2013a). Specimens that were relatively small in scale and/or flexurally dominated were omitted, as they do not represent the real case of deep beams in practice. Figure 6 shows the comparison between the experimental and predicted load capacity using both provisions. The calculated capacities according to both provisions were scattered with different levels of deficiency due to the inherent shortcomings in each provision.

The STM in ACI provisions predicted the failure of either the upper or lower node of the inclined strut for all specimens, which is consistent with the experimental results. The capacity prediction using the STM in ACI 318 (2011) was overestimated and arbitrary, with a mean experimental-to-predicted value of 0.81 and a coefficient of variation (COV) of 34% (Fig. 6(a)). An overestimation was also observed for the steel-reinforced deep beams (Hong and Ha 2012; Reineck and Todisco 2014; Tuchscherer et al. 2014). The overestimated capacities produced by the STM in ACI 318 (2011) for FRP-reinforced deep beams could be explained by the fact that it neglects the effect of concrete softening in the diagonal strut resulting from the presence of high strains in the longitudinal reinforcement (Eq. (5)). Moreover, as shown in Table 3, the prediction for the

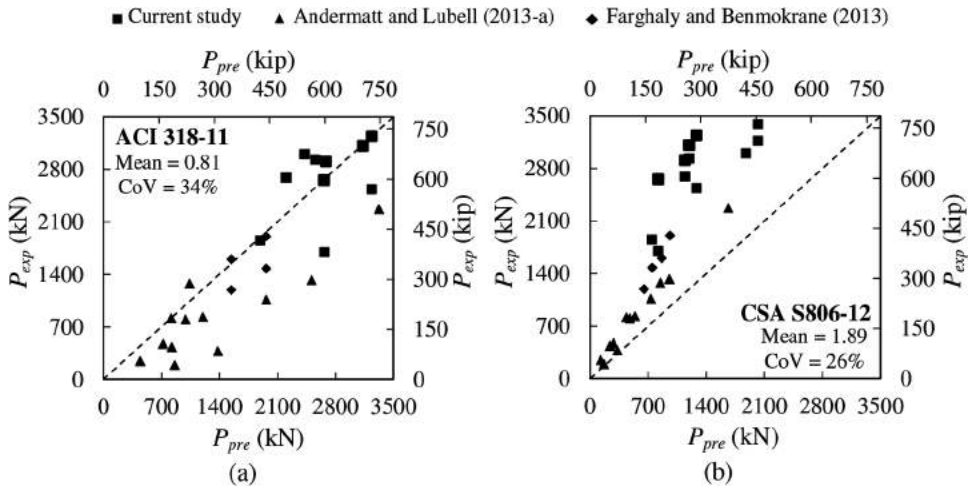


*Fig. 6—Predicted versus experimental capacity using STM in: (a) ACI; and (b) CSA.*

capacity of deep beams with web reinforcement based on ACI 318 (2011) would exceed the capacity of deep beams without web reinforcement by 20%, which is inconsistent with the experimental results in our study (Table 3).

Figure 6(b) shows the conservative prediction based on CSA S806 (2012) for the FRP-reinforced-concrete deep beams tested by Andermatt and Lubell (2013a) and Farghaly and Benmokrane (2013). The level of conservatism was increased for the specimens tested in our study. This level of conservatism was expected as the method exaggerates the negative effect of concrete softening in the diagonal strut due to the longitudinal reinforcement strain through the calculation of $\varepsilon_1$ (Eq. (5)). It is worth mentioning that the maximum strain in the longitudinal reinforcement is limited to 0.002 in the case of steel-reinforced deep beams, but it could reach 0.01 in the case of FRP-reinforced deep beams, which increases $\varepsilon_1$ and, in return, underestimates the efficiency of the diagonal strut. Therefore, it was expected to yield to significantly lower predictions than that of the experiments on deep-beam specimens. The value of the mean ratio of 1.89 indicated the conservative uneconomical prediction with a COV of 26%. Therefore, it can be deduced that the STMs adopted by ACI and CSA do not adequately reflect the capacity of FRP-reinforced deep beams and, consequently, the model must be modified.

## STRUT EFFICIENCY FACTOR

An adequate detailing of truss elements is necessary to ensure the safety of deep beams. This requires that none of the stresses in the STM elements exceed the allowable capacities—yield in steel or rupture in FRP longitudinal reinforcement of the tie or the strut's concrete effective compressive strength. Tie failure—either rupture of the FRP or yielding of the steel bars—can be eliminated by providing an adequate amount of longitudinal reinforcement so as to induce the failure in the struts or nodes (ACI 318-11; CSA S806-12).

Various studies have been conducted to assess the parameters affecting the strut's concrete strength in steel-reinforced deep beams (Reineck and Todisco 2014; Brown and Bayrak 2008). Generally, the design procedure of struts or nodes in the STM has been to combine the effect of strut stress and strain conditions, reinforcement details, and concrete strength (or concrete softening) into one factor, namely the efficiency factor $\beta_s$. Thus, the efficiency factor can be defined as the ratio of stress in the strut $f_{ce}$ to the compressive strength of the concrete $f_c'$; it is calculated as follows

$$\beta_s = \frac{f_{ce}}{0.85 f_c'} = \frac{F_{strut}}{0.85 A_{strut\ (min)} f_c'} \quad (6)$$

The diagonal strut force $F_{strut}$ can be calculated from the truss equilibrium, as shown in Fig. 4 and divided by the minimum cross-sectional area of the strut $A_{strut(min)}$ to determine the maximum stress $f_{ce}$. The minimum cross-sectional area of the strut can be determined by multiplying the width of the diagonal strut $w_{st}$ by the deep beam's breadth ($b$) at both ends of the strut. $w_{st}$ can be easily determined from node geometry, as shown in Fig. 5. The individual effect of each parameter influencing $\beta_s$ for the FRP-reinforced deep beams is discussed in the following section.

### Parameters affecting strut efficiency factor

Figure 7 shows the tendency of the efficiency factor $\beta_s$ with changing parameter values: concrete compressive strength $f_c'$, shear span-depth ratio ($a/d$), and strain of longitudinal reinforcement $\varepsilon_1$ with insignificant web reinforcement effect.

ACI 318 (2011) provisions do not take into account these parameters in calculating $\beta_s$. Moreover, the constant values of $\beta_s$ equal to 0.6 and 0.75—assigned for specimens without and with minimum web reinforcement, respectively—places the prediction in the upper limit of the data cloud, as shown in Fig. 7, leading to an unsafe estimation of the deep beam's capacity. On the other hand, the efficiency factor in CSA S806 (2012) explicitly accounts for $\varepsilon_1$, implicitly considers the effect of $a/d$ through the term $\cot^2\theta$, and does not account for the effect of $f_c'$. Nevertheless, the efficiency factor provided by the CSA provision lies on the lower limit of the data cloud in Fig. 7, leading to a conservative but uneconomic estimation of the deep beam's capacity.

Figure 7(a) shows a relatively clear trend of the negative effect of $f_c'$ on $\beta_s$, although the FRP-reinforced deep beams

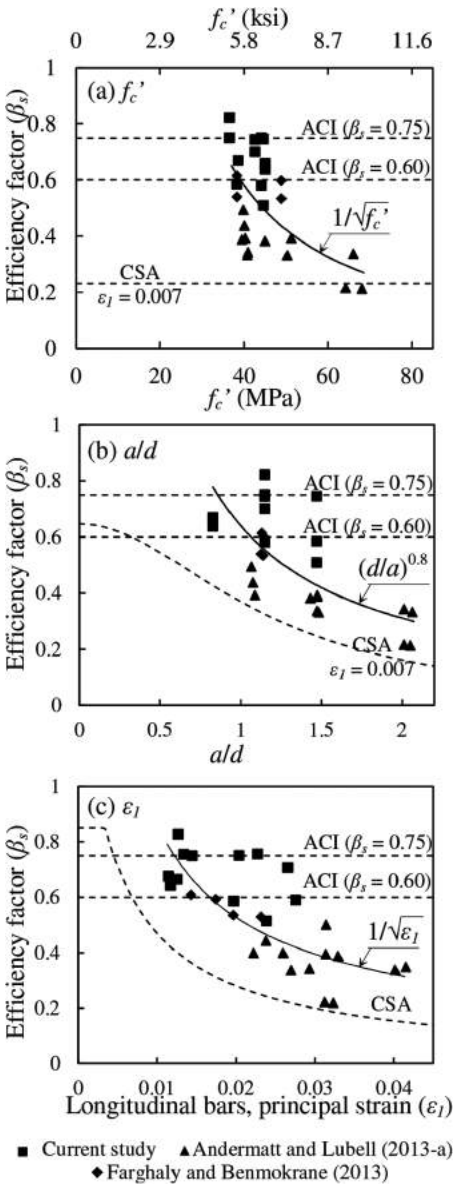


*Fig. 7—Factors affecting measured efficiency factor.*

tested had a limited variety of $f_c'$. This was observed by Andermatt and Lubell (2013a), who attributed that to the limited deformation due to the more brittle nature of the higher-strength concrete, which reduced the efficiency of the diagonal concrete strut. The correlation between the shear strength of deep beams and $a/d$ shown in Fig. 7(b) is predictable (the increased $a/d$ decreased the deep beam's strength), as reported in many studies and most notably in the shear tests conducted by Kani et al. (1979).

In the steel-reinforced deep beams, the concrete softening in the diagonal strut was relatively insignificant because steel-reinforced ties should not reach their yield capacity to satisfy the lower-bound theory. Therefore, the tensile strains in the steel reinforcement were relatively low (less than 0.002). The relatively low elastic modulus of FRP bars, however, induced relatively high strains in the FRP longitudinal reinforcement (compared to the steel), which significantly affected the strength of the diagonal strut and therefore, the efficiency factor.

It should be mentioned that the strain of the longitudinal reinforcement cannot be used directly because the softening of concrete in compression is a function of the principal tensile and compressive strains ($\varepsilon_1$ and $\varepsilon_2$, respectively), while $\varepsilon_2$ is set to 0.002 for crushed concrete in the diagonal strut (Vecchio and Collins 1986). Therefore, the efficiency factor was related to $\varepsilon_1$ rather than the strain of the longitudinal bars, as shown in Fig. 7(c). Farghaly and Benmokrane (2013) reported the ultimate capacity of the tested FRP-reinforced deep beams could be increased solely by increasing the axial stiffness of the longitudinal reinforcement, thereby reducing its strain and enhancing the efficiency of the diagonal strut strength.

### Proposed development of $\beta_s$

Based on the aforementioned discussion, $\beta_s$ is a function of $f_c'$, $a/d$, and $\varepsilon_1$ and can be set in a form as follows

$$\beta_s = z \cdot (f_c')^a \cdot (a/d)^b \cdot (\varepsilon_1)^c \tag{7}$$

where $z$ is constant; and $a$, $b$, and $c$ are the constants representing the correlation between each parameter and $\beta_s$.

Figure 7 shows the results of the least-squares regression performed to identify the correlation of each parameter as –0.5, –0.8, and –0.5 for $a$, $b$, and $c$, respectively. The constant $z$ was set to 0.5 to have the estimation in the lower limit of the data. Therefore, the efficiency factor $\beta_s$ can be calculated as follows

$$\beta_s = 0.5 \frac{1}{\sqrt{f_c'}} \frac{1}{(a/d)^{0.8}} \frac{1}{\sqrt{\varepsilon_1}} \text{ (SI units)} \tag{8a}$$

$$\beta_s = 0.19 \frac{1}{\sqrt{f_c'}} \frac{1}{(a/d)^{0.8}} \frac{1}{\sqrt{\varepsilon_1}} \text{ (Imperial units)} \tag{8b}$$

where $\varepsilon_1$ is given by Eq. 5 and $a/d$ is limited to unity for specimens having a $a/d$ of less than 1.0, to prevent overstressing the strut.

## ASSESSMENT OF PROPOSED MODEL

Figure 8 shows the comparison of the predicted ultimate capacity based on the proposed model (Eq. (8)) versus the experimental results of the current and previous studies of a total of 28 FRP-reinforced deep beams. The predicted capacity was governed by the failure of the diagonal concrete struts in all specimens, which is consistent with the experimental results. The proposed model safely estimated the ultimate capacity with a mean value of 1.22 and a COV of 19%. As illustrated in Fig. 8, however, the model underestimated the experimental capacity of four specimens. Those four specimens had vertical web reinforcement, which would allow for the formation of the two-panel truss model (Fig. (9)) instead of the one-panel truss model shown in Fig. 4. Figure 10 shows the geometry of the nodal regions and the stresses acting on struts and nodal faces. The typical failure mode of specimens with vertical web reinforcement, given in Fig. 11, could support this suggestion. Therefore, it

was essential to examine the two-panel truss model for the tested beams.

### Strain-energy concept

According to Schlaich et al. (1987), the truss model—either the one-panel or two-panel model shown in Fig. 4 and 9, respectively—that contains the least strain energy is likely to be comparable to the experimental results. The strain energy for a truss model is equal to the sum of the strain energy of each member in the STM. To calculate the strain energy for each member, the area under the stress-strain curve such an element is multiplied by its volume. The strain energy for one- and two-panel truss models was calculated from the collected data of FRP-reinforced deep beams to examine the appropriate truss model.

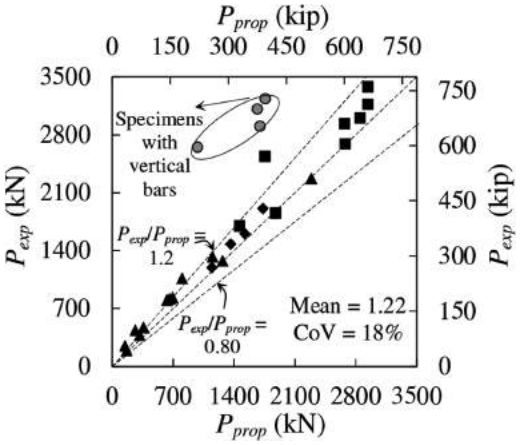


*Fig. 8—Assessment of proposed model (one-panel).*

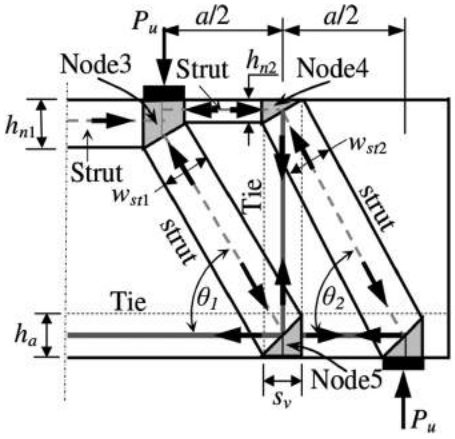


*Fig. 9—Two-panel truss model.*

The stress-strain relationship for concrete and FRP reinforcement was based on the actual material properties for the deep beams tested in our study. For the deep beams in past studies, however, the model developed by Popovics (1973) and modified by Collins and Mitchell (1997) to account for HSC was used to predict the concrete stress-strain curve. FRP reinforcement behaves linearly, so the maximum stresses and strains for the longitudinal reinforcement was calculated from the force acting on the tie and the bar's elastic modulus $E_{frp}$. The maximum strains in the vertical and horizontal web reinforcement were taken as the measured strains during testing. Based on the geometry of the STM (refer to Fig. 4 and 9 for details) and the experimental ultimate capacity, the force in each truss member and its stress and strain in either the one- or two-panel truss model were determined.

All struts were assumed to be prismatic-shaped to calculate their volumes, considering that the dispersion of compression in a bottle-shaped strut produces fewer stresses at the middle of the strut than that at its ends. These lower stresses compensate for the greater cross-sectional area at the middle of the strut; therefore, assuming a prismatic-shaped strut was convenient. The area of the diagonal struts at both ends were calculated by multiplying strut width (as in Fig. 5 and 10) by the width of the deep beam $b$. The strut volumes were then calculated by multiplying the strut area by strut length. The total area of the longitudinal reinforcement was used in calculating tie volume. For the two-panel truss model, all the vertical and horizontal reinforcement within the deep beam's shear span were included in determining the volume of the web reinforcement.

Basically, the strain energy can also be represented as the area under the load-deflection curve, which was used to verify the strain-energy calculation. Figure 12 shows the relationship between the least strain energy from the one- and two-panel truss models and that from the area under load-deflection curve. It clearly shows that the calculation procedure defined by Schlaich et al. (1987) resulted in an acceptable prediction of the strain energy, with a mean value of 1.12 and a COV of 15%.

Figure 13 shows the data for the strain-energy ratio (ratio of one-panel to two-panel strain energies). Accordingly, the one-panel truss model would be used if the strain energy ratio were less than one. Figure 13 depicts that the strain-energy ratio for all tested FRP-reinforced deep beams resulted in the use of the one-panel truss model, except for the four specimens with vertical web reinforcement, which

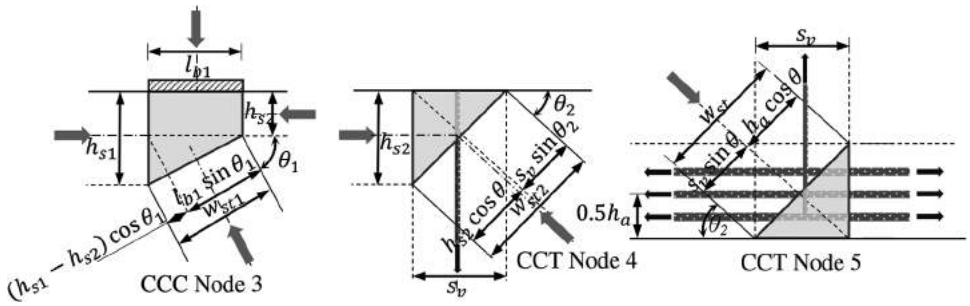


*Fig. 10—Two-panel STM nodal geometry.*

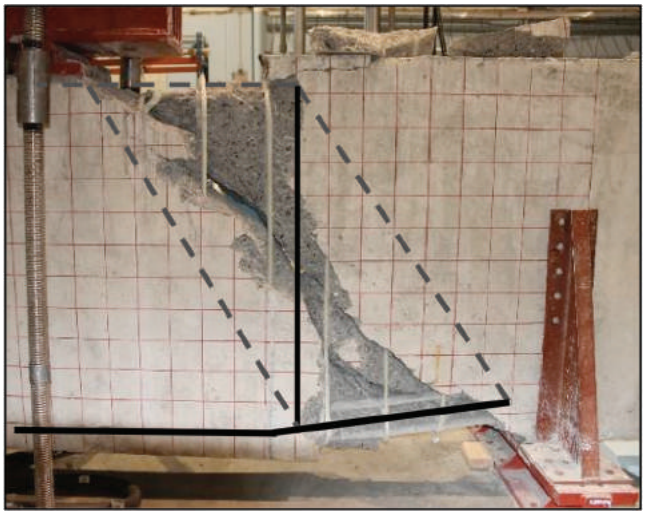

*Fig. 11—Formation of two-panel STM in tested deep beams with vertical stirrups.*

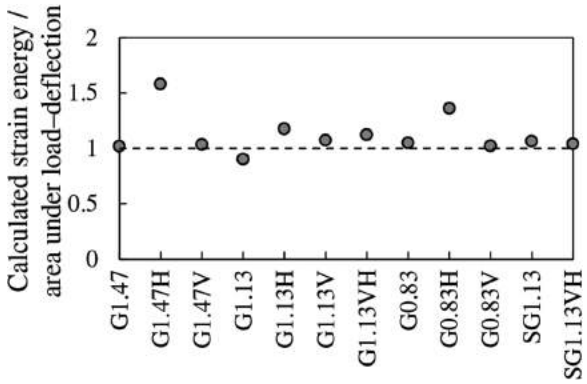


*Fig. 12—Calculated strain energy versus area under load-deflection curve.*

acted as a vertical tie between the two struts and led to using the two-panel truss model.

Applying the two-panel solution for specimens with vertical web reinforcement using the proposed truss model resulted in more accurate estimation of the specimen's capacity, as shown in Fig. 14. The mean value and COV for the experimental-to-proposed capacity were 1.17% and 15%, respectively. The two-panel solution was also applied to predict the capacity according to the STM in ACI 318 (2011) and CSA S806 (2012), but it insignificantly improved the predicted values (refer to Table 3).

Further verification for the proposed model was conducted by comparison to the steel-reinforced deep beams, showing its applicability. As long as the steel bars were properly anchored, no yield in the longitudinal steel reinforcement occurred, and the failure was induced by concrete crushing at the struts. Therefore, the proposed model was used to calculate the capacity of 172 steel-reinforced deep beams gathered from the literature (Clark 1951; Foster and Gilbert 1998; Oh and Shin 2001; Aguilar et al. 2002, Zhang and Tan 2007; Alcocer and Uribe 2008; Mihaylov et al. 2010; Tuchscherer et al. 2011; and Birrcher et al. 2014). The beams were of comparable size to the deep beams currently used in practice, therefore small-scale specimens with a total

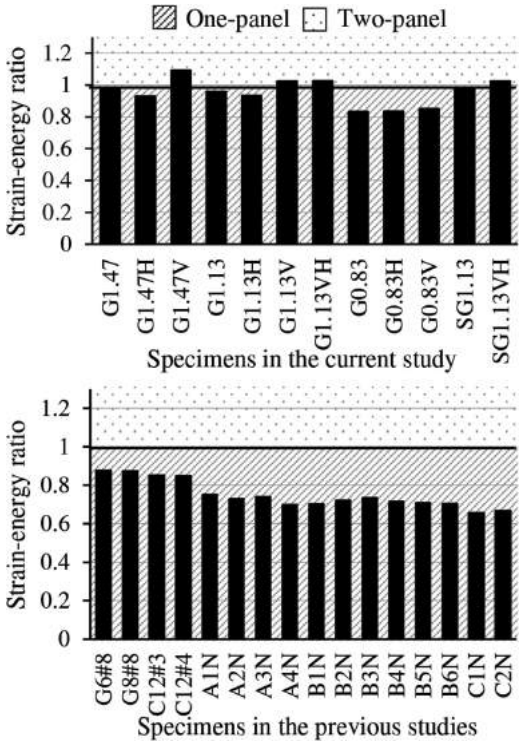


*Fig. 13—Strain-energy ratio for tested FRP-reinforced deep beams.*

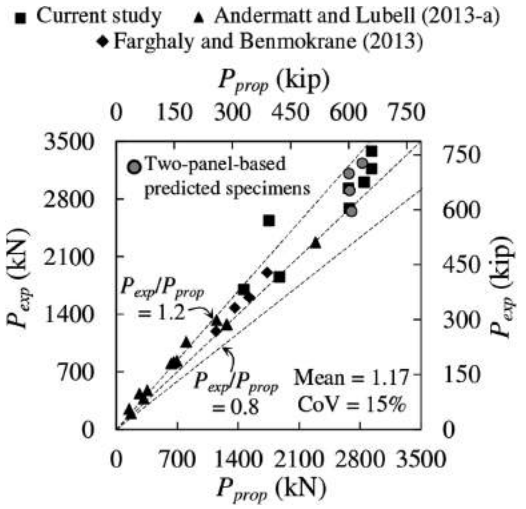


*Fig. 14—Assessment of proposed model based on one- and two-panel truss models.*

height of less than 500 mm (19.7 in.) were not considered. The deep beams included in the assessment had $a/d$ values ranging from 0.27 to 2.20, concrete strengths ranging from 13.8 to 120 MPa (2.0 to 17.4 ksi), and various combinations of web reinforcement. Beams that were described as having a failure mode other than shear (anchorage and/or flexural failure) were not included in the assessment.

Figure 15(a) shows calculated capacities using the proposed model versus the reported experimental capacity. The proposed model was capable of predicting the ultimate capacity of steel-reinforced deep beams with a mean experimental-to-predicted value of 1.09 and a COV of 22%. Figures 15(b) and (c) show the predicted capacity using the

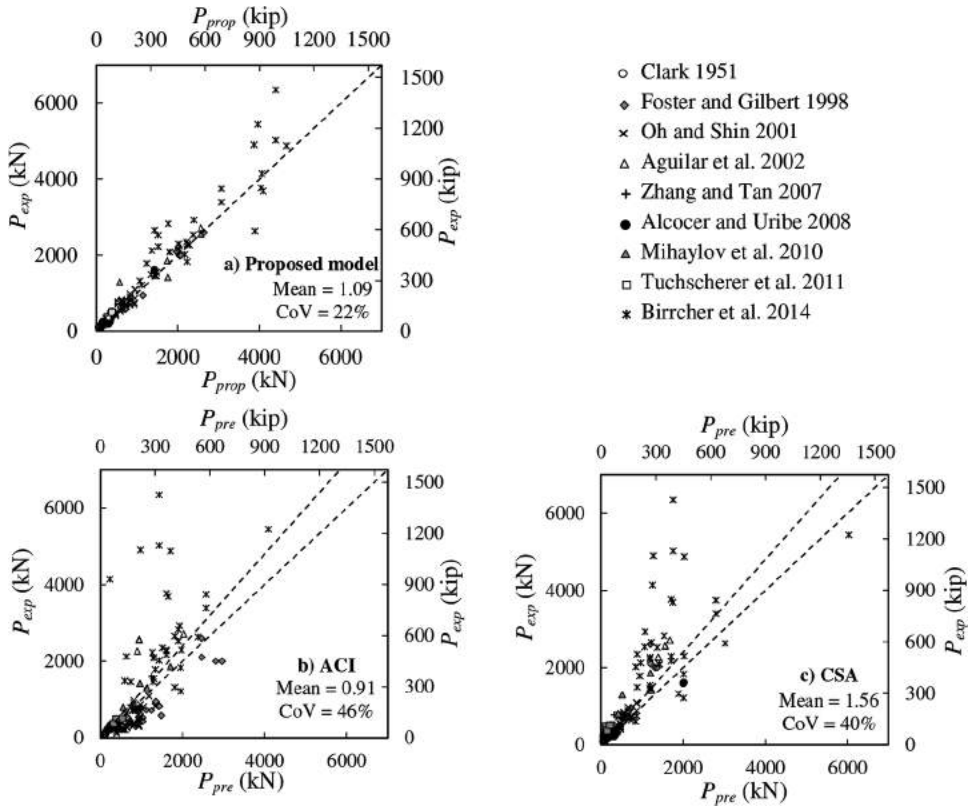


*Fig. 15—Predicted versus experimental capacity for steel-reinforced deep beams.*

STMs in ACI 318 (2011) and CSA A23.3 (2014), respectively. Consistent with the predicted results for the FRP-reinforced deep beams, ACI 318 (2011) overestimated the capacity of the specimens and CSA A23.3 (2014) produced conservative but uneconomic estimations of capacity.

## CONCLUSIONS

The main purpose of this research was to assess the accuracy of the STMs in design provisions (ACI and CSA) and to quantify the efficiency factor with the affecting parameters. The efficiency factor in ACI 318 (2011) overestimated the ultimate capacity. The efficiency factor in CSA S806 (2012), however, underestimated the ultimate capacity, which could lead to uneconomic designs. These results reveal the importance of having a more rational model for estimating the efficiency factor. Therefore, a new model for the strut efficiency factor—accounting for the concrete compressive strength, shear span-depth ratio, and strain in the longitudinal reinforcement was proposed. The strain-energy concept was used to identify the development of either a one- or two-panel truss model. The procedure for strain-energy calculation was verified by comparing the results to the area under the load-deflection curves for the tested deep beams. The two-panel truss model was found to be appropriate for the specimens with vertical web reinforcement. Nevertheless, the authors recommend the use of the one-panel truss model because it yields an acceptable level of conservatism. The proposed model was compared against the available FRP-reinforced deep beams and to steel-reinforced deep beams. The proposed model produced safe estimations for capacity predictions with an acceptable level of conservatism.

## AUTHOR BIOS

**Khaled Mohamed** *is a Doctoral Candidate in the Department of Civil Engineering, University of Sherbrooke, Sherbrooke, QC, Canada. He received his BSc and MSc degrees from Assiut University, Assiut, Egypt. His research interests include the structural analysis, design, and testing of concrete structures reinforced with fiber-reinforced polymers.*

**Ahmed Sabry Farghaly** *is a Postdoctoral Fellow in the Department of Civil Engineering at the University of Sherbrooke. His research interests include nonlinear analysis of reinforced concrete structures and behavior of structural concrete reinforced with fiber-reinforced polymers.*

**Brahim Benmokrane**, *FACI, is Professor of civil engineering and NSERC Research Chair in FRP Reinforcement for Concrete Infrastructure and Tier-1 Canada Research Chair in Advanced Composite Materials for Civil Structures in the Department of Civil Engineering at the University of Sherbrooke. He is a member of ACI Committee 440, Fiber-Reinforced Polymer Reinforcement.*

## ACKNOWLEDGMENTS

The experimental study was conducted with funding from the Tier-1 Canada Research Chair in Advanced Composite Materials for Civil Structures and Natural Sciences and Engineering Research Council of Canada (NSERC-Industry Research Chair program). The assistance of the technical staff of the new Canadian Foundation for Innovation (CFI) structural lab at the University of Sherbrooke's Department of Civil Engineering is also acknowledged.

## REFERENCES

ACI Committee 318, 2011, "Building Code Requirements for Structural Concrete and Commentary (ACI 318-11)," American Concrete Institute, Farmington Hills, MI, 503 pp.

ACI Committee 440, 2006, "Guide for the Design and Construction of Concrete Reinforced with FRP Bars (ACI 440.1R-06)," American Concrete Institute, Farmington Hills, MI, 44 pp.

Aguilar, G.; Matamoros, A. B.; Parra-Montesinos, G. J.; Ramirez, J. A.; and Wight, J. K., 2002, "Experimental Evaluation of Design Procedures for Shear Strength of Deep Reinforced Concrete Beams," *ACI Structural Journal*, V. 99, No. 4, July-Aug., pp. 539-548.

Alcocer, S. M., and Uribe, C. M., 2008, "Monolithic and Cyclic Behavior of Deep Beams Designed Using Strut-and-Tie Models," *ACI Structural Journal*, V. 105, No. 3, May-June, pp. 327-337.

Andermatt, M. F., and Lubell A. S., 2013a, "Behavior of Concrete Deep Beams Reinforced with Internal Fiber-Reinforced Polymer—Experimental Study," *ACI Structural Journal*, V. 110, No. 4, July-Aug., pp. 585-594.

Andermatt, M. F., and Lubell A. S., 2013b, "Strength Modeling of Concrete Deep Beams Reinforced with Internal Fiber-Reinforced Polymer," *ACI Structural Journal*, V. 110, No. 4, July-Aug., pp. 595-605.

Birrcher, D. B.; Tuchscherer, R. G.; Huizinga, M.; and Bayrak, O., 2014, "Depth Effect in Deep Beams," *ACI Structural Journal*, V. 111, No. 4, July-Aug., pp. 731-740. doi: 10.14359/51687002

Brown, M. D., and Bayrak, O., 2006, "Minimum Transverse Reinforcement for Bottle-Shaped Struts," *ACI Structural Journal*, V. 103, No. 6, Nov.-Dec., pp. 813-821.

Brown, M. D., and Bayrak, O., 2008, "Design of Deep Beams Using Strut-and-Tie Models—Part II: Design Recommendations," *ACI Structural Journal*, V. 105, No. 4, July-Aug., pp. 405-413.

Clark, A. P., 1951, "Diagonal Tension in Reinforced Concrete Beams," *ACI Journal Proceedings*, V. 48, No. 10, Oct., pp. 145-156.

Collins, M. P., and Mitchell, D., 1997, "Prestressed Concrete Structures," *Response Publications*, Canada, 766 pp.

CSA A23.3-14, 2014, "Design of Concrete Structures," Canadian Standards Association, Mississauga, ON, Canada, 295 pp.

CSA S806-12, 2012, "Design and Construction of Building Components with Fiber-Reinforced Polymers," Canadian Standards Association, Mississauga, ON, Canada, 208 pp.

Farghaly, A. S., and Benmokrane, B., 2013, "Shear Behavior of FRP-Reinforced Concrete Deep Beams without Web Reinforcement," *Journal of Composites for Construction*, ASCE, V. 17, No. 6, pp. 04013015.1-10.

Foster, S. J., and Gilbert, R. I., 1998, "Experimental Studies on High-Strength Concrete Deep Beams," *ACI Structural Journal*, V. 95, No. 4, July-Aug., pp. 382-390.

Hong, S.-G., and Ha, T., 2012, "Effective Capacity of Diagonal Strut for Shear Strength of Reinforced Concrete Beams without Shear Reinforcement," *ACI Structural Journal*, V. 109, No. 2, Mar.-Apr., pp. 139-148.

Kani, M. W.; Huggins, M. W.; Kani, G.; and Wittkopp, R. R., 1979, *Kani on Shear in Reinforced Concrete*, University of Toronto Press, Toronto, ON, Canada, 225 pp.

MacGregor, J. G., 1997, *Reinforced Concrete, Mechanics and Design*, third edition, Prentice Hall, Upper Saddle River, NJ, 939 pp.

Mihaylov, B. I.; Bentz, E. C.; and Collins, M. P., 2010, "Behavior of Large Deep Beams Subjected to Monotonic and Reversed Cyclic Shear," *ACI Structural Journal*, V. 107, No. 6, Nov.-Dec., pp. 726-734.

Oh, J.-K., and Shin, S.-W., 2001, "Shear Strength of Reinforced High-Strength Concrete Deep Beams," *ACI Structural Journal*, V. 98, No. 2, Mar.-Apr., pp. 164-173.

Popovics, S., 1973, "A Numerical Approach to the Complete Stress-Strain Curve of Concrete," *Cement and Concrete Research*, V. 3, No. 5, pp. 583-599. doi: 10.1016/0008-8846(73)90096-3

Reineck, K.-H., and Todisco, L., 2014, "Database of Shear Tests for Non-Slender Reinforced Concrete Beams without Stirrups," *ACI Structural Journal*, V. 111, No. 6, Nov.-Dec., pp. 1363-1372. doi: 10.14359/51686820

Schlaich, J.; Schäfer, K.; and Jennewein, M., 1987, "Toward a Consistent Design of Structural Concrete," *PCI Journal*, V. 32, No. 3, May-June, pp. 74-150.

Tuchscherer, R.; Birrcher, D.; Huizinga, M.; and Bayrak, O., 2011, "Distribution of Stirrups across Web of Deep Beams," *ACI Structural Journal*, V. 108, No. 1, Jan.-Feb., pp. 108-115.

Tuchscherer, R. G.; Birrcher, D. B.; Williams, C. S.; Deschenes, D. J.; and Bayrak, O., 2014, "Evaluation of Existing Strut-and-Tie Methods and Recommended Improvements," *ACI Structural Journal*, V. 111, No. 6, Nov.-Dec., pp. 1451-1460. doi: 10.14359/516869926

Vecchio, F. J., and Collins, M. P., 1986, "The Modified Compression-Field Theory for Reinforced Concrete Elements Subjected to Shear," *ACI Journal Proceedings*, V. 83, No. 2, Mar.-Apr., pp. 219-231.

Zhang, N., and Tan, K.-H., 2007, "Size Effect in RC Deep Beams: Experimental Investigation and STM Verification," *Journal of Engineering Structures*, V. 29, No. 12, pp. 3241-3254. doi: 10.1016/j.engstruct.2007.10.005